

Phase diagram of a superconductor / ferromagnet bilayer

M. Lange,* M. J. Van Bael, and V. V. Moshchalkov
*Laboratory for Solid State Physics and Magnetism,
Nanoscale Superconductivity and Magnetism Group,
K.U. Leuven, Celestijnenlaan 200 D, 3001 Leuven, Belgium*
(Dated: November 21, 2018)

The magnetic field (H) - temperature (T) phase diagram of a superconductor is significantly altered when domains are present in an underlying ferromagnet with perpendicular magnetic anisotropy. When the domains have a band-like shape, the critical temperature T_c of the superconductor in zero field is strongly reduced, and the slope of the upper critical field as a function of T is increased by a factor of 2.4 due to the inhomogeneous stray fields of the domains. Field compensation effects can cause an asymmetric phase boundary with respect to H when the ferromagnet contains bubble domains. For a very inhomogeneous domain structure, $T_c \propto H^2$ for low H and $T_c \propto H$ for higher fields, indicating a dimensional crossover from a one-dimensional network-like to a two-dimensional behavior in the nucleation of superconductivity.

PACS numbers: 74.25.Dw 74.25.Ha 74.76.Db 75.70.Kw

I. INTRODUCTION

In hybrid superconductor / ferromagnet (SC/FM) bilayers the FM modifies quite substantially the superconducting properties of the SC layer. In particular, strong vortex pinning was reported recently for superconducting films covering arrays of ferromagnetic dots with in-plane^{1,2,3} and out-of-plane magnetization,^{4,5} and for continuous SC/FM bilayers.^{6,7,8,9,10} Theoretical investigations showed that supercurrents and vortices can be induced in the SC by the stray field of the FM,^{11,12,13,14,15,16} and that the domain structure of soft FM's can be influenced by the presence of the SC.¹⁷ Furthermore, Radovic et al. predicted the appearance of the so-called π -phase state in SC/FM multilayers, where the phase of the superconducting order parameter ψ shifts by π when crossing a ferromagnetic layer.¹⁸ Recently the existence of the π -phase state was confirmed by observing sharp cusps in the temperature dependence of the critical current in SC/FM/SC junctions.¹⁹ Earlier experiments were performed in order to find the π -phase state by measuring the predicted oscillatory dependence of the critical temperature T_c of SC/FM multilayers on the FM layer thickness d_{fm} .^{20,21,22,23} However, the results of these experiments were not conclusive, because the nonmonotonic $T_c(d_{fm})$ behavior could also appear due to the presence of magnetically "dead" layers at the SC/FM interfaces.²¹

The theory of the anomalous $T_c(d_{fm})$ dependence is based on the Usadel equations²⁴ describing the proximity effect of FM and SC layers, but neglecting a possible influence of the domains in the FM. In this manuscript we will show that an inhomogeneous stray field B_{stray} produced by the domain structure of a FM can actually also lead to a significant change in T_c . To demonstrate this effect, we measure T_c as a function of the perpendicularly applied magnetic field H of a Pb film on top of a Co/Pt multilayer with perpendicular magnetic anisotropy. In this sample the proximity effect

is suppressed by an amorphous Ge layer between Pb and Co/Pt. The domain structure in the Co/Pt multilayer can consist of stable band or bubble domains. The FM layer can also be in a single domain state, depending on the preceding magnetization procedure, as was shown in a recent study of the vortex pinning in this system.¹⁰ Due to field cancellation effects between H and B_{stray} , and due to the suppression of ψ by B_{stray} , $T_c(H)$ can be controlled by changing the microscopic domain structure.

II. MAGNETIC PROPERTIES OF THE Co/Pt MULTILAYER

The properties of the Co/Pt multilayer have been described before.¹⁰ Briefly, the multilayer has a [Co(0.4 nm)/Pt(1.0 nm)]₁₀ structure on a 2.8 nm Pt base layer on a Si/SiO₂ substrate. The magnetic properties were characterized by the magneto-optical Kerr effect (MOKE) and magnetic force microscopy (MFM), revealing that the sample has perpendicular magnetic anisotropy. Fig. 1 shows the magnetization M_{fm} of the Co/Pt multilayer measured by MOKE, normalized to the saturation magnetization M_{sat} , as a function of the magnetic field H applied perpendicular to the surface. The loop has an almost rectangular shape with $\mu_0 H_n = 60$ mT, $\mu_0 H_c = 93$ mT, and $\mu_0 H_s = 145$ mT, where H_n , H_c and H_s are the nucleation, coercive and saturation field, respectively, and μ_0 is the permeability of the vacuum.

Using different magnetization procedures, one can produce different stable domain patterns in the sample. For instance, after out-of-plane demagnetization, band domains are observed by MFM, see Fig. 1(b). Stable bubble domains with local magnetic moments \mathbf{m} either pointing up ($m_z > 0$) or down ($m_z < 0$) perpendicular to the sample surface can be created by applying a negative field of -1 T, sweeping H to a positive value between H_n and

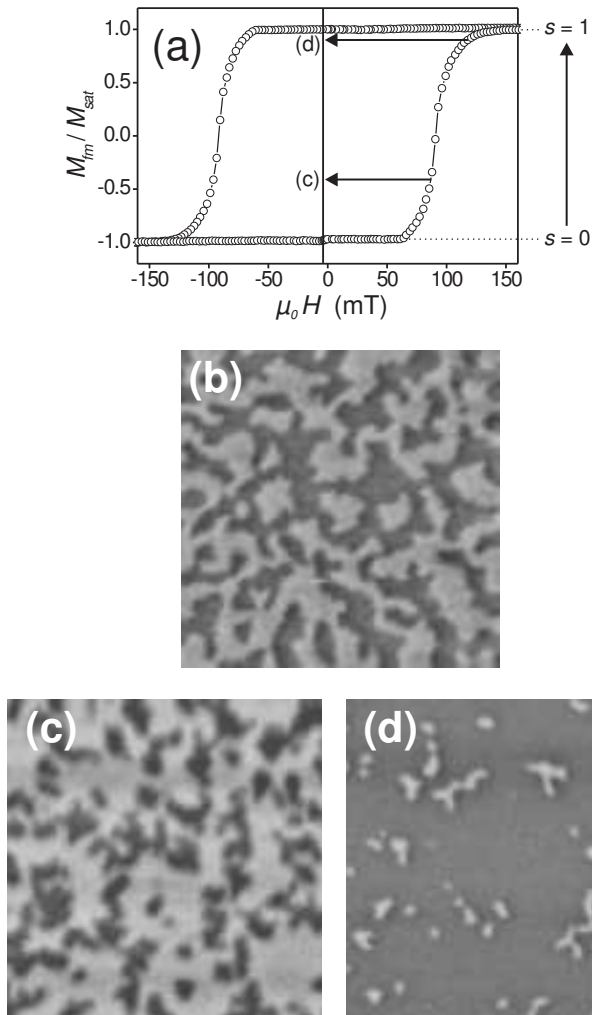


FIG. 1: Magnetic properties of the Co/Pt multilayer: (a) Hysteresis loop measured by magneto-optical Kerr effect with H perpendicular to the sample surface. MFM images ($5 \times 5 \mu\text{m}^2$) show that the domain structure of the sample consists of band domains after out-of-plane demagnetization (b), bubble domains in the $s = 0.3$ (c) and $s = 0.93$ (d) states.

H_s , and then removing H . The parameter s , which gives the fraction of magnetic moments that are pointing up ($m_z > 0$) to the total amount of magnetic moments, is used to describe the different remanent magnetic states obtained after this magnetization procedure. The value of s can be found from the MFM images by dividing the dark area ($m_z > 0$) by the total area, or from measurements of M_{fm} as will be described later.

The lateral size of the domain structures can be estimated from the MFM images. The typical diameter of the bubble domains is about ~ 300 nm. The same value is obtained for the average width of the band domains. Although the magnetic moments of the Co/Pt multilayer are equally distributed between up- and down-directions in both the demagnetized and the $s = 0.5$ state, there are distinct differences between these two domain states:

In the demagnetized state the lateral size of the domain is larger (because band domains are extended in one direction). Note also that in the demagnetized state, the boundary between domains with magnetization pointing up and down is well defined, but not straight: several sharp corners of different angles can be seen. No MFM images could be obtained for the $s = 0.5$ state, caused by the difficult magnetization procedure due to the steep slope of the $M_{fm}(H)$ curve, see Fig. 1(a). However, from the image of the $s = 0.3$ state, see Fig. 1(c), one can observe that the domain walls are less sharp defined than in the demagnetized state.

III. PHASE BOUNDARY OF THE SUPERCONDUCTING FILM

After characterizing the properties of the FM, a 10 nm Ge film, a 50 nm Pb film and a 30 nm Ge capping layer are subsequently evaporated on the Co/Pt multilayer at a substrate temperature of 77 K. The amorphous Ge film between Pb and Co/Pt is insulating at low temperatures, so that the proximity effects between Pb and Co/Pt are suppressed.

The upper critical field H_{c2} of bulk type-II SCs is given by²⁵

$$\mu_0 H_{c2}(T) = \frac{\Phi_0}{2\pi\xi^2(T)}. \quad (1)$$

with $\Phi_0 = 2.068 \text{ mT } \mu\text{m}^2$ the superconducting flux quantum, $\xi(T) = \xi(0)/\sqrt{1 - T/T_{c0}}$ the temperature dependent coherence length in the dirty limit, and T_{c0} the critical temperature at zero field. Hence, the linear slope of H_{c2} as a function of temperature is only determined by the coherence length ξ .

$H_{c2}(T)$ can behave differently when the geometry of the SC is changed, e.g. for thin films with thickness $w < \xi(T)$. While eq. 1 is still valid for thin type-II superconducting films with H applied perpendicular to the sample surface, T_c for parallel H is given by²⁶

$$T_c(H) = T_{c0} \left[1 - \frac{\pi^2 \xi^2(0) w^2}{3\Phi_0^2} \mu_0^2 H^2 \right], \quad (2)$$

with T_{c0} the zero-field critical temperature. In fact, this formula also gives the phase boundary of a mesoscopic line in perpendicular field, because the cross section, exposed to the applied field, is the same for a film of thickness w in parallel H and for a mesoscopic line in perpendicular H .²⁷ For multiply connected mesoscopic lines, $T_c(H)$ can show an even more complex behavior due to fluxoid quantization effects.²⁸

The phase boundary of the SC/FM bilayer was measured in a Quantum Design superconducting quantum interference device (SQUID) magnetometer with H applied perpendicular to the surface. Fig. 2 shows the data obtained in two field cooled measurements of the total magnetization $M = M_{fm} + M_{sc}$ (M_{sc} is the magnetization of the SC) at the applied field of $\mu_0 H = 0.5 \text{ mT}$,

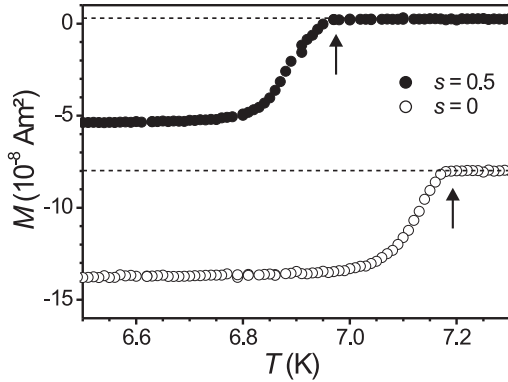
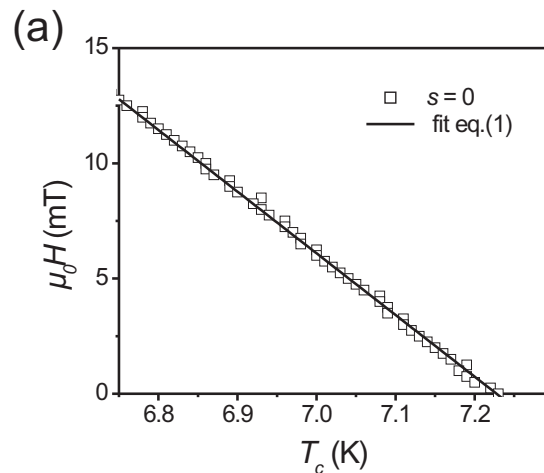


FIG. 2: Field cooled $M(T)$ measurements of the hybrid SC/FM bilayer in $\mu_0 H = 0.5$ mT with the Co/Pt multilayer in the $s = 0.5$ (●) and $s = 0$ (○) states. The arrows indicate T_c .

after the samples were brought in the $s = 0.5$ and $s = 0$ states. Above T_c , M has a constant value for both states, given by the contribution of the FM M_{fm} , from which s can be derived. When the sample is cooled through T_c , a diamagnetic response of the SC appears. These kinds of measurements were used to determine $T_c(H)$ as the temperature where M starts to deviate from M_{fm} . Repeating these measurements at several applied fields $|H| < 25$ mT did not change the offset M_{fm} above T_c , implying an unchanged domain state.

A. $T_c(H)$ with magnetized FM

The phase boundary for the $s = 0$ state (all $m_z < 0$) obtained by several $M(T)$ measurements in varying fields is shown in Fig. 3(a). A linear behavior of the phase boundary is observed, which can be fitted by eq. 1 with $\xi(0) = (41.2 \pm 0.2)$ nm and $T_{c0} = (7.227 \pm 0.002)$ K. This implies that in this state, the FM has no influence on the superconducting film, because both the linear behavior and the values of T_{c0} and $\xi(0)$ are in good agreement with those of pure Pb films.²⁹ It is important to note that the temperature dependence of $\xi(T) = \xi(0)/\sqrt{1 - T/T_{c0}}$ derived for this domain state is the same for all domain states, since we are always dealing with the same Pb film. Let us consider the magnetic stray field B_{stray} of a homogeneously magnetized film in the $s = 0$ state, schematically drawn in Fig. 3(b). B_{stray} has its largest amplitude at the sample boundary and is negligible above the center of the FM. Intuitively this can be understood by considering the stray field of a single magnetic dipole in the center of the sample: The negative field above the dipole is compensated by the returning positive stray field of the surrounding magnetic dipoles. Therefore, the main central part of the superconductor is only weakly influenced by B_{stray} , and the measured $T_c(H)$ curve resembles the



(b)

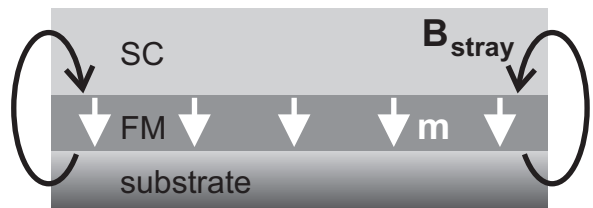


FIG. 3: (a) Magnetic field - temperature phase diagram of the superconducting Pb film covering the Co/Pt multilayer. Before measuring $T_c(H)$, the Co/Pt multilayer was brought into the $s = 0$ state. (b) Schematic drawing of the stray field B_{stray} when the FM is in the $s = 0$ state.

one of a single Pb film.

B. $T_c(H)$ with demagnetized FM

The phase boundary for the demagnetized state, corresponding to the MFM image shown in Fig. 1(b), is shown in Fig. 4(a). In this state, T_{c0} is suppressed to (7.048 ± 0.002) K. Moreover, the phase boundary still shows a linear behavior, but with a slope increased by a factor of 2.4. The difference between the phase boundaries in the demagnetized and the $s = 0$ state can be attributed to the influence of the stray field B_{stray} , suppressing the order parameter in the superconductor above $T = 7.048$ K. The coherence length at this temperature is $\xi = 260$ nm. This means that superconductivity nucleates when the value of ξ becomes smaller than approximately the width of the band domains. The nucleation first takes place in regions of the Pb film where the effective field in the z -direction $\mu_0 H_{eff,z} = \mu_0 H_z + B_{stray,z}$ is minimum. The confinement of these superconducting nuclei leads to the different $T_c(H)$ dependence compared to the magnetized state. Aladyskhin *et al.* have very recently calculated the $T_c(H)$

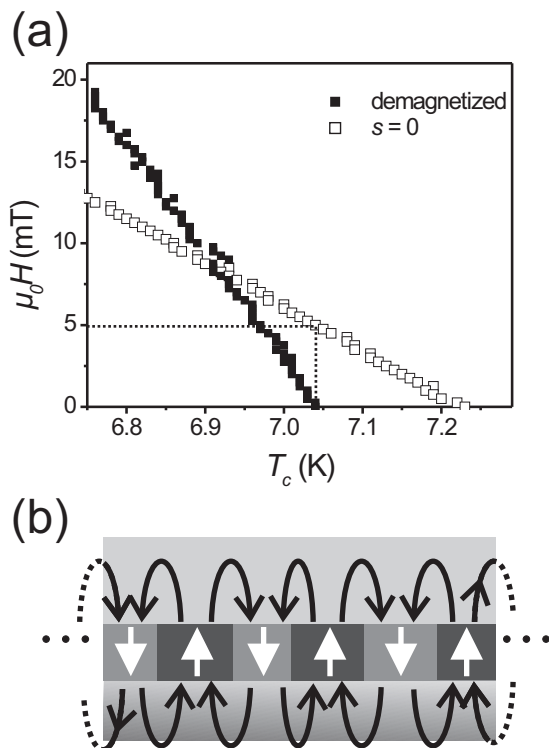


FIG. 4: (a) Magnetic field - temperature phase diagram of the superconducting Pb film covering the Co/Pt multilayer. The Co/Pt multilayer was demagnetized before measuring $T_c(H)$. As a reference we have added the phase boundary of the $s = 0$ state. The dashed lines are guides to the eye. (b) Schematic drawing of the stray field B_{stray} when the FM has been demagnetized.

phase boundary of similar systems as the one that is experimentally investigated here in the framework of the linearized Ginzburg-Landau equation.³⁰ They found, in agreement with our experimental result, that the upper critical field of a superconducting film can have very unusual temperature dependencies when a single domain wall or periodic domain structures are present in a ferromagnetic film that is in contact with the superconductor. Based on these considerations, we can conclude that the increased slope of the $T_c(H)$ curve may be related to the specific domain pattern in the demagnetized state. The MFM image in Fig. 1(b) shows an equal contrast above all bright or dark domains, indicating that B_{stray} is rather homogeneous above the domains, and inhomogeneous above the domain walls, which define some sharp corners. From calculations of the upper critical field of mesoscopic superconducting structures, e.g., triangles or squares, it is well known that the nucleation of superconductivity takes place first in the corners of these structures.^{31,32} Therefore, when trying to calculate the $T_c(H)$ phase boundary in order to explain the increased slope, one should take into account these corners formed by the domain walls. This could be done by expanding the one-dimensional model used by Aladyshkin *et al*³⁰ to

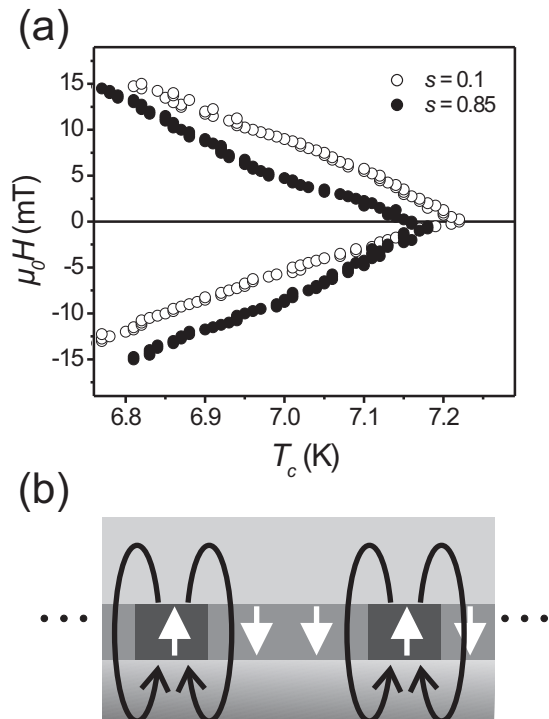


FIG. 5: (a) Magnetic field - temperature phase diagrams of the superconducting Pb film covering the Co/Pt multilayer. Before measuring $T_c(H)$, the Co/Pt multilayer was brought into the $s = 0.1$ and $s = 0.85$ states.

two dimensions.

C. $T_c(H)$ with bubbles in the FM

The phase boundary shown in Fig. 5(a) is obtained when the Co/Pt multilayer contains bubble domains. Fig. 3 and Fig. 4 are symmetric with respect to H , i.e., T_c is the same for positive or negative H , but the presence of the bubble domains causes an *asymmetry of T_c with respect to H* . For bubbles having positive magnetic moments, i.e. $s < 0.5$, a higher T_c is observed for positive H than for corresponding negative H , whereas for bubbles containing negative magnetic moments ($s > 0.5$), T_c is higher for negative H . Moreover, both $T_c(H)$ curves shown in Fig. 5(a) show a non-linear behavior with bumps in the field ranges around $|\mu_0 H| \approx 5 - 10$ mT. To explain the asymmetric $T_c(H)$ curves, let us assume that the sample contains bubble domains with $m_z > 0$ in a matrix of magnetic moments with $m_z < 0$, as shown in Fig. 5(b): $B_{stray,z}$ is positive above the bubbles and negative between them. A positive H in the z -direction compensates the negative $B_{stray,z}$ between the bubbles and enhances $B_{stray,z}$ above them, while a negative H has the opposite effect: it enhances $B_{stray,z}$ between the bubbles and compensates $B_{stray,z}$ above them. The important point that causes the asymmetric phase boundary is that the absolute value of $B_{stray,z}$ is larger above

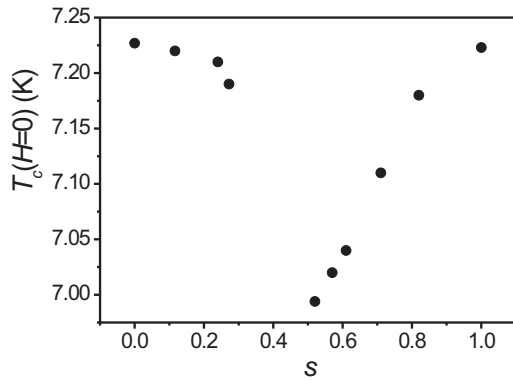


FIG. 6: Dependence of the critical temperature at zero field $T_c(H=0)$ on the parameter s . The minimum value of T_c is observed for $s = 0.5$.

the $m_z > 0$ regions (bubbles) compared to the $m_z < 0$ regions (between the bubbles). When the sample is cooled in positive H , superconductivity can nucleate at higher temperatures in the area between the bubbles (where $B_{stray,z} < 0$), compared to cooling the sample in the corresponding negative H , where the nucleation takes place in the areas above the bubbles. Note that qualitatively similar non-linear $T_c(H)$ curves as those presented in Fig. 5(a) have also been predicted by Aladyshkin *et al.*³⁰

The critical temperature of the superconductor decreases when the bubble domains have larger density. To illustrate this effect, Fig. 6 shows the dependence of $T_c(H = 0)$ on the parameter s . A clear minimum of T_c is observed around $s = 0.5$, which indicates that this domain state has the largest value of the stray field of all investigated domain structures. Note that T_c of the $s = 0.5$ state is even lower than T_c of the demagnetized state, emphasizing the inhomogeneous character of the $s = 0.5$ state. The phase boundary of this domain state will be discussed in the next section.

D. $T_c(H)$ with the FM in the $s = 0.5$ state

The phase boundary of the SC with the FM in the $s = 0.5$ state is shown in Fig. 7. In this domain state, B_{stray} has a more inhomogeneous character than in the demagnetized state. For a discussion of the differences between these two domain states we refer to section II. $T_c(H)$ follows a non-linear behavior, in contrast to the demagnetized and the $s = 0$ states. $T_c(H)$ for the $s = 0.5$ state can not be described by eq. 1, but rather by eq. 2 in fields $\mu_0 H < 15$ mT, see the fit in Fig. 7(b). This indicates that in the $s = 0.5$ state the regions where superconductivity nucleates can be considered as superconducting strips with a width $w \leq \xi(T)$, forming a sort of a superconducting network. When fitting the $T_c(H)$ curve

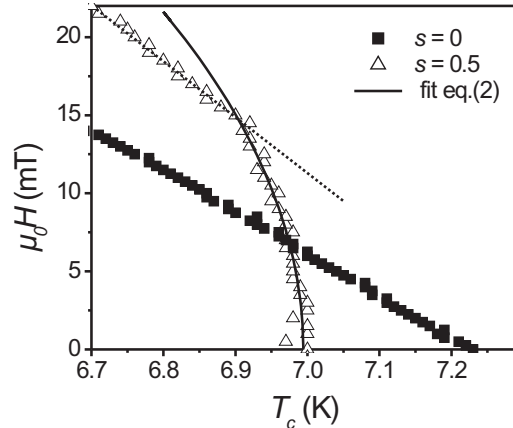


FIG. 7: Magnetic field - temperature phase diagrams of the superconducting Pb film covering the Co/Pt multilayer. Before measuring $T_c(H)$, the Co/Pt multilayer was brought into the $s = 0.5$ state. As a reference the phase boundary of the $s = 0$ state is added. The dashed line is a guide to the eye.

using eq. 2 and $\xi(0) = 41.2$ nm (from the phase boundary for $s = 0$), we obtain values of $w = (213 \pm 6)$ nm and $T_{c0} = (6.994 \pm 0.003)$ K. The value of w determined from this fit can be compared with the typical bubble domain size of ~ 300 nm. For $\mu_0 H > 15$ mT and $T < 6.90$ K, $T_c(H)$ shows a crossover from the one-dimensional network like to a two-dimensional linear behavior, because the assumption $w < \xi(T)$ for eq. 2 is no longer fulfilled. This is in agreement with the value of $\xi(6.90 \text{ K}) = 194$ nm.

IV. CONCLUSION

In conclusion, the phase boundary between the normal and the superconducting state of FM/SC bilayers has been found to be strongly dependent on the domain structure in the FM. The stray field B_{stray} of these domains can lead to a significant decrease of T_c in zero applied field, but, on the other hand, it can also enhance T_c in applied fields. It has been demonstrated that the presence of bubble domains leads to the formation of the field-polarity dependent asymmetric phase boundaries $T_c(H)$ with respect to H , due to compensation effects between H and B_{stray} . For a specific inhomogeneous domain structure, the $T_c(H)$ phase boundary shows a crossover from a one-dimensional to a two-dimensional nucleation behavior.

Acknowledgments

The authors thank L. Van Look, K. Temst and G. Güntherodt for help with sample preparation, J. Swerts for MOKE measurements and Y. Bruynseraede for fruitful discussions. This work was supported by the Fund

for Scientific Research - Flanders (Belgium) (F.W.O.-Vlaanderen), by the Belgian IUAP and the European ESF "VORTEX" Programs, and by the Research Fund K.U.Leuven GOA. ML and MJVB are Postdoctoral Research Fellows of the F.W.O.-Vlaanderen.

-
- * Electronic address: martin.lange@fys.kuleuven.ac.be
- ¹ Y. Otani, B. Pannetier, J. P. Nozières, and D. Givord, *J. Magn. Magn. Mat.* **126**, 622 (1993).
 - ² J. I. Martín, M. Vélez, J. Nogués, and I. K. Schuller, *Phys. Rev. Lett.* **79**, 1929 (1997).
 - ³ M. J. Van Bael, K. Temst, V. V. Moshchalkov, and Y. Bruynseraede, *Phys. Rev. B* **59**, 14674 (1999).
 - ⁴ D. J. Morgan and J. B. Ketterson, *Phys. Rev. Lett.* **80**, 3614 (1998).
 - ⁵ M. J. Van Bael, L. Van Look, K. Temst, M. Lange, J. Bekaert, U. May, G. Güntherodt, V. Moshchalkov, and Y. Bruynseraede, *Physica C* **332**, 12 (2000).
 - ⁶ L. N. Bulaevskii, E. M. Chudnovsky, and M. P. Maley, *Appl. Phys. Lett.* **76**, 2594 (2000).
 - ⁷ A. García-Santiago, F. Sánchez, M. Varela, and J. Tejada, *Appl. Phys. Lett.* **77**, 2900 (2000).
 - ⁸ X. X. Zhang, G. H. Wen, R. K. Zheng, G. C. Xiong, and G. J. Lian, *Europhys. Lett.* **56**, 119 (2001).
 - ⁹ Y. I. Bespyatykh, W. Wasilevski, M. Gajdek, I. P. Nikitin, and S. A. Nikitov, *Phys. Solid State* **43**, 1827 (2001).
 - ¹⁰ M. Lange, M. J. Van Bael, V. V. Moshchalkov, and Y. Bruynseraede, *Appl. Phys. Lett.* **81**, 322 (2002).
 - ¹¹ I. K. Marmorkos, A. Matulis, and F. M. Peeters, *Phys. Rev. B* **53**, 2677 (1996).
 - ¹² M. V. Milosevic, S. V. Yampolskii, and F. M. Peeters, *Phys. Rev. B* **66**, 024515 (2002).
 - ¹³ I. F. Lyuksyutov and V. L. Pokrovsky, *Phys. Rev. Lett.* **81**, 2344 (1998).
 - ¹⁴ S. Erdin, I. F. Lyuksyutov, V. L. Pokrovsky, and V. M. Vinokur, *Phys. Rev. Lett.* **88**, 017001 (2002).
 - ¹⁵ Y. I. Bespyatykh and W. Wasilevski, *Phys. Solid State* **43**, 224 (2001).
 - ¹⁶ E. B. Sonin, *Pis'ma Zh. Tekh. Phys.* **14**, 1640 (1988) [*Sov. Tech. Phys. Lett.* **14**, 714 (1988)]; R. Laiho, E. Lähderanta, E. B. Sonin, and K. B. Traito, *Phys. Rev. B* **67**, 144522 (2003).
 - ¹⁷ A. I. Buzdin and L. N. Bulaevskii, *Sov. Phys. JETP* **67**, 576 (1988).
 - ¹⁸ Ž. Radovic, M. Ledvij, L. Dobrosavljević-Grujić, A. I. Buzdin, and J. R. Clem, *Phys. Rev. B* **44**, 759 (1991).
 - ¹⁹ V. V. Ryazanov, V. A. Oboznov, A. Y. Rusanov, A. V. Veretennikov, A. A. Golubov, and J. Aarts, *Phys. Rev. Lett.* **86**, 2427 (2001).
 - ²⁰ J. S. Jiang, D. Davidovic, D. H. Reich, and C. L. Chien, *Phys. Rev. Lett.* **74**, 314 (1995).
 - ²¹ T. Mühge, N. N. Garif'yanov, Y. V. Goryunov, G. G. Khal-iullin, L. R. Tagirov, K. Westerholt, I. A. Garifullin, and H. Zabel, *Phys. Rev. Lett.* **77**, 1857 (1996).
 - ²² J. Aarts, J. M. E. Geers, E. Bruck, A. A. Golubov, and R. Coehoorn, *Phys. Rev. B* **56**, 2779 (1997).
 - ²³ L. Lazar, K. Westerholt, H. Zabel, L. R. Tagirov, Y. V. Goryunov, N. N. Garif'yanov, and I. A. Garifullin, *Phys. Rev. B* **61**, 3711 (2000).
 - ²⁴ K. Usadel, *Phys. Rev. Lett.* **25**, 507 (1970).
 - ²⁵ M. Tinkham, *Introduction to superconductivity* (McGraw-Hill, Inc., New York, ed. 2, 1996).
 - ²⁶ M. Tinkham, *Phys. Rev.* **129**, 2413 (1963).
 - ²⁷ V. V. Moshchalkov, L. Gielen, C. Strunk, R. Jonckheere, X. Qiu, C. Van Haesendonck, and Y. Bruynseraede, *Nature* **373**, 319 (1995).
 - ²⁸ V. Bruyndoncx, C. Strunk, V. V. Moshchalkov, C. Van Haesendonck, and Y. Bruynseraede, *Europhys. Lett.* **36**, 449 (1996).
 - ²⁹ L. Van Look, PhD thesis, K.U.Leuven, Belgium (2002).
 - ³⁰ A. Y. Aladyshkin, A. I. Buzdin, A. A. Fraerman, A. S. Mel'nikov, D. A. Ryzhov, and A. V. Sokolov, *Domain wall superconductivity in hybrid superconductor-ferromagnetic structures* (2003), (unpublished), cond-mat/0305520.
 - ³¹ V. M. Fomin, J. T. Devreese, and V. V. Moshchalkov, *Europhys. Lett.* **42**, 553 (1998); **46**, 118 (1999).
 - ³² V. A. Schweigert and F. M. Peeters, *Phys. Rev. B* **60**, 3084 (1999).